Supplement of: Aerosol Size Distribution and New Particle Formation in High Mountain Environments: A Comparative Study at Monte Cimone and Jungfraujoch GAW Stations

Martina Mazzini et al.

S1 Data Availability

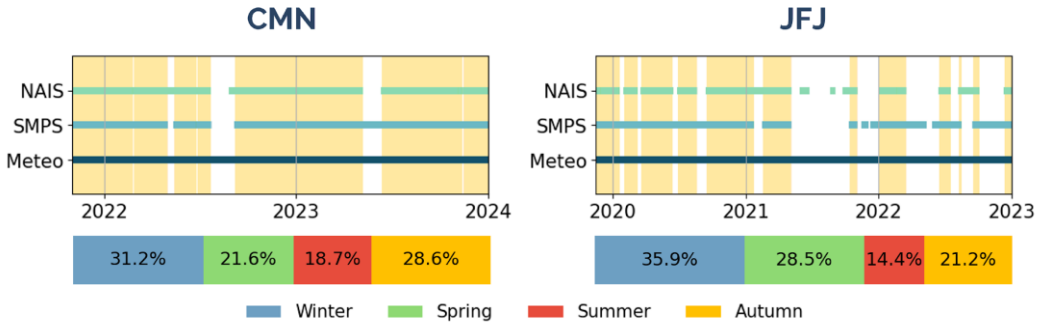

Figure S1. Data coverage at CMN and JFJ for NAIS, SMPS, and meteorological data. The yellow area indicates the common operational period for both NAIS and SMPS at each station. The percentage of seasons refers to these overlapping periods.

S2 Correction applied to NAIS data

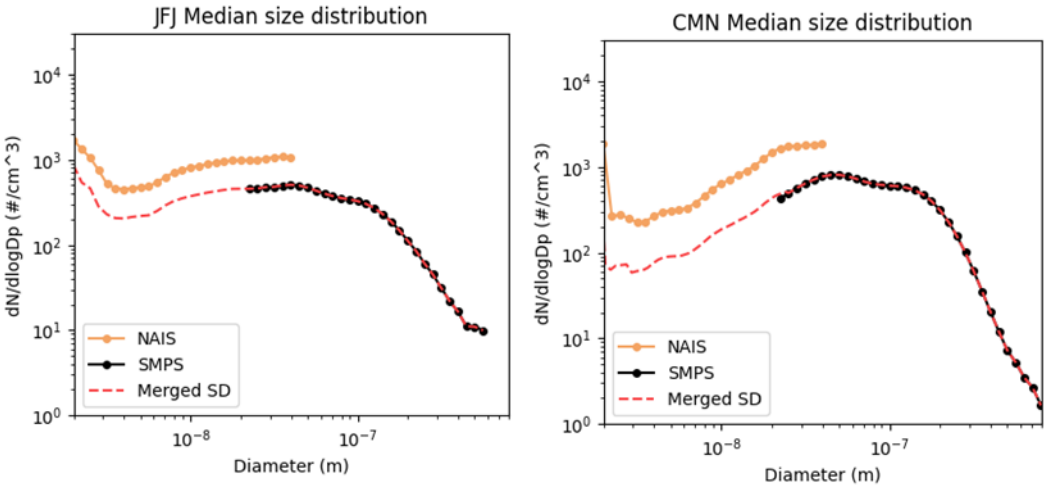

Figure S2. Median PNSD derived by NAIS and SMPS instruments at JFJ and CMN stations. The red dotted line represent the final merged PNSD, after NAIS data correction.

S3 Calculation of Growth and Formation Rates, Coagulation and Condensation Sink

To characterize NPF events, we calculated both the particle formation rate J and the growth rate GR for particles within the 2.5–7 nm size range. The formation rate $J_{2.5}$ represents the flux of particles growing beyond the 2.5 nm threshold and was determined based on the aerosol general dynamic equation (Kulmala et al., 2012). This equation accounts for the time-dependent change in particle number concentration and includes terms for both coagulation losses and particle growth:

$$J_{2.5} = \frac{dN_{[2.5,7)}}{dt} + CoagS_{2.5-7} \cdot N_{[2.5-7)} + \frac{GR_{2.5-7}}{(7-2.5)nm} \cdot N_{[2.5-7)}$$

In this formulation, $N_{[2.5-7)}$ is the concentration of particles between 2.5 and 7 nm, $CoagS_{2.5-7}$ represents the coagulation sink for this size range, and $GR_{2.5-7}$ denotes the growth rate of the particles.

The coagulation sink describes the rate at which particles are lost due to coagulation with other particles, effectively removing them from the nucleation mode. It is calculated by integrating over all particle size bins and considering the collision rates between particles of different sizes. The coagulation sink $CoagS(d_p)$ for a given particle diameter d_p is defined as:

$$CoagS(d_p) = \sum_{d_{p_i} \geq d_p} K\left(d_p, d_{p_i}\right) \cdot N\left(d_{p_i}\right) \cdot \Delta d_{p_i}$$

where $K\left(d_p, d_{p_i}\right)$ is the coagulation coefficient between diameters d_p and d_{p_i}, $N\left(d_{p_i}\right)$ is the number concentration of particles with diameter d_{p_i}, and Δd_{p_i} is the differential diameter.

The average coagulation sink $\langle CoagS \rangle_{2.5-7}$ for diameters between 2.5 and 7 nm was calculated as:

$$\langle CoagS \rangle_{2.5-7} = \frac{1}{N} \sum_{d_p \in [2.5nm, 7nm]} CoagS(d_p)$$

where N is the number of diameters d_p considered within the range of 2.5 and 7 nm.

The $GR_{2.5-7}$ was determined using the maximum concentration method (Kulmala et al., 2012), which identifies the time at which the peak particle concentration occurs. First, the particle size distribution data were smoothed using a rolling median filter and further refined using a Gaussian filter to reduce noise. This allowed for accurate detection of the time of maximum concentration for particles within the 2.5 and 7 nm size range. These time points were then plotted against the corresponding particle diameters, and a linear least-squares fit was applied to the data. The slope of this line was used to calculate the $GR_{2.5-7}$:

$$GR_{2.5-7} = \frac{\Delta d_{p_{[2.5-7]}}}{\Delta t}$$

where $\Delta d_{p_{[2.5-7]}}$ is the change in particle diameter (from 2.5 to 7 nm), and Δt is the corresponding time interval. The GR, expressed in nm/h, provides a measure of how quickly particles grow during NPF events. The growth rate was a value retrieved only for the day of new particle formation events, one for each nucleation day.

In addition to the coagulation sink, the condensation sink CS was also considered, which quantifies the rate at which condensing vapors, such as sulfuric acid, are scavenged by the pre-existing aerosol population. This is an important factor as it influences the availability of condensable vapors that drive particle growth. The CS is calculated as (Kulmala et al., 2012):

$$CS = 4\pi D \sum_i \left(N_i \cdot \beta\left(d_{p_i}, T, P, D, M_{H_2SO_4}\right) \cdot d_{p_i}\right)$$

where D is the diffusion coefficient of the condensing vapor, which we consider to be sulfuric acid in air, N_i is the number concentration of aerosol particles, d_{p_i} is the particle diameter, and β is the deposition coefficient. The number concentration is derived from the aerosol number size distribution, and the binary diffusivity and deposition coefficients are determined based on the ambient conditions. The summation is performed over all diameter bins of the aerosol size distribution.

S4 PNSD seasonality

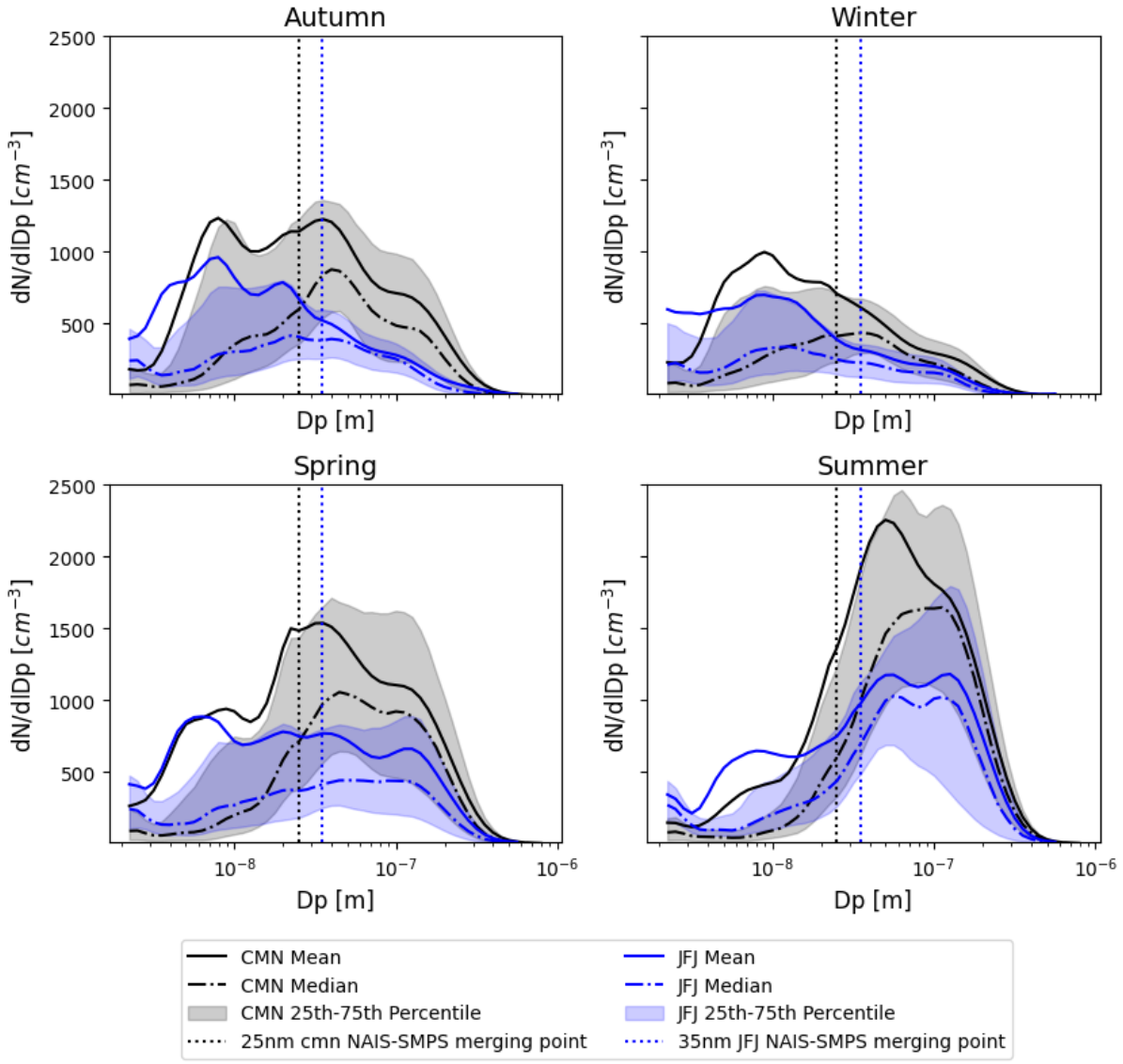

Figure S3. Seasonal variation of particle size distribution at the CMN (black) and JFJ (blue) stations. The dashdotted lines represent the median, while the solid lines indicate the mean particle size distribution. The shaded area encompasses the interquartile range, reflecting the 25th to 75th percentiles. The vertical dashed lines mark the merging points between the scaled NAIS size distribution and the SMPS size distribution (25 nm at CMN and 35 nm at JFJ).

S5 Ions Seasonal diurnals

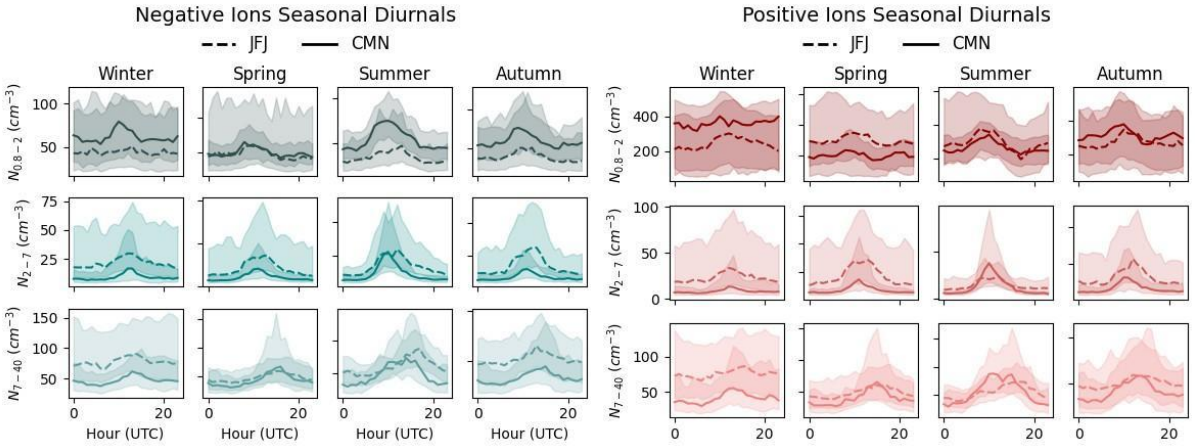

66

67 **Figure S4.** Diurnal variation of negative (left) and positive (right) number concentrations across three modes (0.8–2 nm, 2–
68 7 nm and 7–40 nm) for each season at the CMN and JFJ stations. All times are in UTC.

69 The diurnal behaviour of the ions is similar at both stations as shown in Fig. S3. At JFJ, the negative
70 cluster ions exhibit peak activity predominantly in the early afternoon, around 13:00 to 14:00, during
71 the winter and summer seasons. During spring and autumn, the peak occurs earlier, at around
72 12:00. Negative intermediate ions follow a similar pattern, maintaining consistent peak times around
73 midday, generally between 12:00 and 13:00, with minor seasonal shifts. However, negative large ions
74 show a tendency to peak later in the afternoon, especially in spring and summer, where their peak
75 times extend from 14:00 to as late as 17:00. Positive cluster ions closely follow the diurnal pattern of
76 negative cluster ions, peaking between 12:00 and 14:00 in most seasons, except for autumn, when the
77 peak occurs at 10:00. Meanwhile, positive intermediate and large ions display more delayed peak
78 times, particularly for the latter, where the maximum is observed as late as 16:00 during spring and
79 summer.

80 At CMN, the diurnal behavior of ions shifts to earlier hours compared to JFJ. Negative cluster ions
81 peak between 08:00 and 10:00 during most seasons. Negative intermediate ions peaks also occur at
82 earlier hours, after the maximum cluster ions peaks, between 10:00 and 12:00. Finally, large negative
83 ions at CMN display a tendency to peak in the early to mid-afternoon, from 13:00 to 16:00, with
84 particularly delayed peaks in spring and autumn. The behavior of positive cluster ions is like that of
85 negative cluster ions, except the large positive ions that typically reach their maximum later in the
86 day, between 13:00 and 15:00.

87

88

S6 In-Cloud Conditions and Particle Size Distribution

A closer examination of the particle size distribution when RH exceeds 97% shows an anomalous increase in sub-10 nm particles (Fig. S4), the origin of which remains uncertain. Further investigation is needed to determine whether this signal reflects a real atmospheric process or an instrumental artifact. At the same time we can see clearly how in-cloud scavenging is responsible for the observed decrease in CCN (50–800 nm).

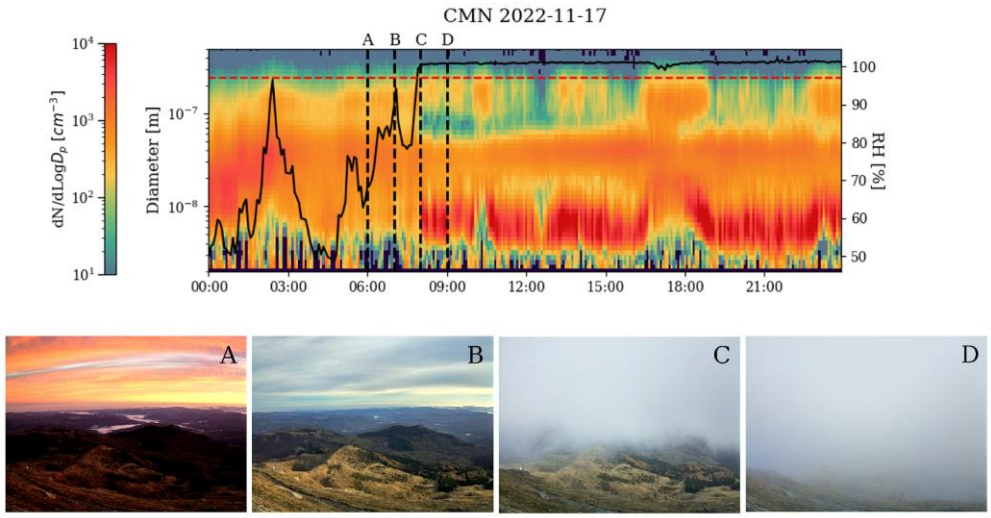

Figure S5. Case study from 2022-11-17 at CMN. The solid black line represents the relative humidity (RH) variation throughout the day, while the red dotted line marks the 97% RH threshold, above which the station is considered to be in cloud. Points A, B, C, and D correspond to 6:00, 7:00, 8:00, and 9:00, respectively, illustrating the transition from out-of-cloud to in-cloud conditions, as observed via the station's weather camera.

S7 NPF event frequency across classification methods

	Class IA	Class IB	Class II	Not Event	Undefined
CMN	9.3%	12.4%	10.2%	61.2%	7.0%
JFJ	2.7%	4.9%	5.8%	50.0%	36.6%

Table S1. Event statistics at CMN and JFJ according to Dal Maso et al. (2005) classification.

	Regional	Transported	Bursts	Not Event
CMN	22.3%	13.3%	14.0%	50.3%
JFJ	3.8%	9.8%	15.0%	71.4%

104 **Table S2.** Event statistics at CMN and JFJ according to Dada et al. (2017) classification.

	Intense	Moderate	Weak	Negligible
CMN	11.0%	17.4%	30.8%	40.9%
JFJ	4.6%	12.8%	31.5%	51.2%

105 **Table S3.** Event statistics at CMN and JFJ according to Nanoparticle ranking analysis (Aliaga et al., 2023).

106